Steady state response of a granular layer to a moving load – A discrete model

A.S.J. Suiker
Delft University of Technology, Koiter Institute Delft/Faculty of Aerospace Engineering,
P.O. Box 5058, 2600 GB Delft, The Netherlands

A.V. Metrikine
Delft University of Technology, Faculty of Civil Engineering and Geosciences,
P.O. Box 5048, 2600 GA Delft, The Netherlands

R. de Borst
Delft University of Technology, Koiter Institute Delft/Faculty of Aerospace Engineering,
P.O. Box 5058, 2600 GB Delft, The Netherlands

This paper discusses the steady state response of a rigidly supported, granular layer to a moving load. Accordingly, the dynamic behaviour of a ballast layer under an instantaneous train axle passage is simulated, where the rigid support reflects a substratum that is much stiffer than the ballast layer, e.g. ballast in a concrete railway tunnel or on a concrete railway foundation. The discrete nature of the layer is captured via a 9-cell square lattice. After deriving the equations of motion for the lattice, the long-wave approximation of the equations of motion is compared with the equations of motion for a continuum model. This leads to relations between the macroscopic constitutive parameters of the continuum and the microscopic constitutive parameters of the discrete lattice. Next, the boundary value problem is formulated and solved. The influence by the particle size, the damping characteristics and the load velocity on the layer response is demonstrated via a parametric study.

Key words: **Railway track, ballast behaviour, discrete lattice, moving load, wave propagation.**

1 Introduction

In railway transport, the continuous demand for capacity increase as well as for more extensive mobility networks automatically sets up a critical assessment with respect to the effectiveness of currently operating and newly-built railway lines. In order to meet the high standards regarding effectiveness, in many countries train cruising speeds of 200 km/h and more have been employed. The track response of these high-speed lines has a typical dynamic character. Hence, for a reliable prediction of track safety and track deterioration, it is necessary to utilise advanced track models that cover the relevant vibration effects and wave propagation phenomena.
Most dynamic track models developed during the last three decades rely on the continuum theory (see for example, Fryba [1972], Labra [1975], Dieterman and Metrikine [1996], Dieterman and

Metrikine [1997], Suiker et al. [1998]). Although these models have disclosed many important features of high-speed railway systems, the nature of the continuum theory prohibits that such models properly simulate the discrete behaviour of the ballast layer. The discrete behaviour of ballast becomes especially significant when a ballast layer is supported by a stiffer substratum of concrete (i.e. railway tunnels, railway foundations) or rock, which is the result of high-frequency wave reflections at the ballast-substratum interface that may perturb the ballast particles individually (Suiker et al. [1999a], Suiker et al. [1999b]).

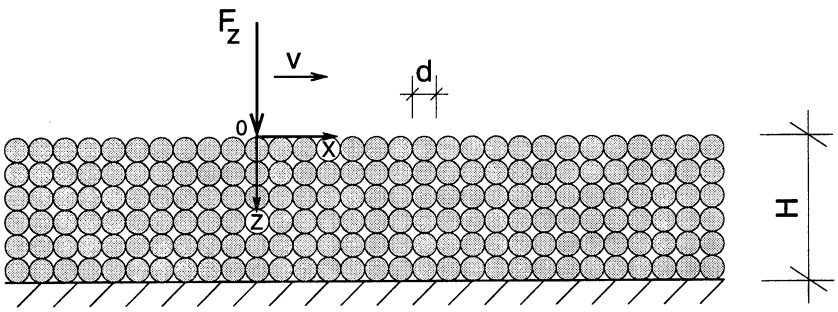

Fig. 1. Moving load on a layer of circular particles.

In this paper, the dynamic response of a layer of discrete ballast particles to a moving load is investigated. The moving load represents an axle loading of a high-speed train vehicle. The discrete layer is modelled by a square lattice, which consists of cells that are mutually connected via elastic longitudinal springs. Here, the cell distance relates to the particle size. An elastic material law for the lattice springs is justified, since under an instantaneous axle passage the response of a railway track is mainly reversible. After deriving the mathematical framework that describes the boundary value problem, a parametric study is carried out. The parametric study illustrates how the discrete layer response is influenced by the ballast particle size, the ballast damping characteristics and the load velocity.

2 Governing equations for a discrete lattice

In Fig. 1 we have depicted a discrete layer of thickness H, which consists of equal-sized, circular particles of diameter d. The layer is subjected to a vertical load F_z, that moves with velocity v along the layer surface. The internal layer geometry and the mechanical interactions by the particles are modelled by a square lattice. In the interior of the layer, the square lattice is constructed of an inner cell with coordinates (m,n) that is connected via axial longitudinal springs K^{n}_{axi} to 4 neighbouring mid-side cells at distance d, and via diagonal longitudinal springs K^{n}_{dia} to 4 neighbouring edge cells at distance $\sqrt{2}d$ (Fig. 2). The lattice cells have two degrees of freedom, which are the displacements in x-direction and z-direction, $u_i = \{u_x, u_z\}$. The centre of the cells corresponds to the centre of gravity

of the particles, while the cell distance d corresponds to the particle diameter. By neglecting the body forces, the equations of motion for the inner cell (m,n) of the square lattice can be derived as

$$
\begin{aligned}
M\ddot{u}_x^{(m,n)} &= \frac{1}{2}K_{axi}^n[-4u_x^{(m,n)} + 2u_x^{(m+1,n)} + 2u_x^{(m-1,n)}] \\
&+ \frac{1}{2}K_{dia}^n[u_z^{(m+1,n+1)} + u_z^{(m-1,n-1)} - u_z^{(m+1,n-1)} - u_z^{(m-1,n+1)} \\
&-4u_x^{(m,n)} + u_x^{(m+1,n+1)} + u_x^{(m+1,n-1)} + u_x^{(m-1,n+1)} + u_x^{(m-1,n-1)}] \\
M\ddot{u}_z^{(m,n)} &= \frac{1}{2}K_{axi}^n[-4u_z^{(m,n)} + 2u_z^{(m,n+1)} + 2u_z^{(m,n-1)}] \\
&+ \frac{1}{2}K_{dia}^n[u_x^{(m+1,n+1)} + u_x^{(m-1,n-1)} - u_x^{(m+1,n-1)} - u_x^{(m-1,n+1)} \\
&-4u_z^{(m,n)} + u_z^{(m+1,n+1)} + u_z^{(m+1,n-1)} + u_z^{(m-1,n-1)} + u_z^{(m-1,n+1)}]
\end{aligned}
\tag{1}
$$

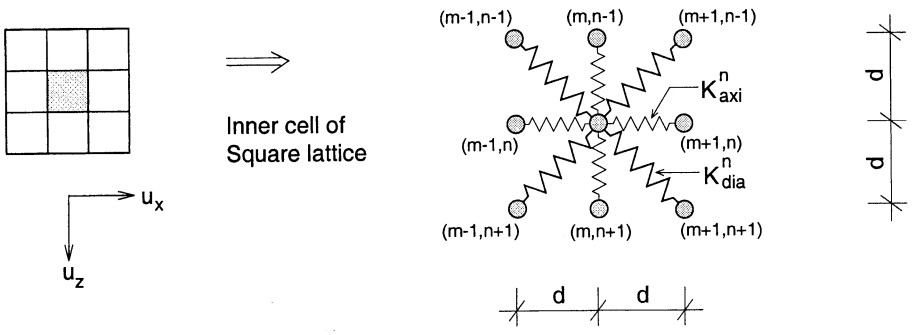

Fig. 2. Inner cell of square lattice

where M is the mass of the inner cell and $\{\ddot{u}_x^{(m,n)}, \ddot{u}_z^{(m,n)}\}$ are the accelerations in x-direction and z-direction. The dot on top of the degrees of freedom designates the full derivative with respect to time. The derivation procedure leading to (1), is explained in more detail in (Suiker et al. [2000]). At the free boundary of the layer ($z = 0$), the square lattice is characterised by a boundary cell that is connected to three neigbouring mid-side cells at distance d, and to two neighbouring edge cells at distance $\sqrt{2}d$ (Fig. 3.). In fact, the boundary cell can be retrieved from the inner cell when the three

neighbouring cells on top of the inner cell are omitted. Hence, the equations of motion for the boundary cell $(m,0)$ may be directly derived from Eq.(1), yielding

$$\begin{aligned} M\ddot{u}_x^{(m,0)} &= \frac{1}{2}K_{axi}^n[-4u_x^{(m,0)} + 2u_x^{(m+1,0)} + 2u_x^{(m-1,0)}] \\ &+ \frac{1}{2}K_{dia}^n[-2u_x^{(m,0)} + u_x^{(m+1,1)} + u_x^{(m-1,1)} + u_z^{(m+1,1)} - u_z^{(m-1,1)}] \\ M\ddot{u}_z^{(m,0)} &= \frac{1}{2}K_{axi}^n[-2u_z^{(m,0)} + 2u_z^{(m,1)}] \\ &+ \frac{1}{2}K_{dia}^n[-2u_z^{(m,0)} + u_z^{(m+1,1)} + u_z^{(m-1,1)} + u_x^{(m+1,1)} - u_x^{(m-1,1)}] \end{aligned} \tag{2}$$

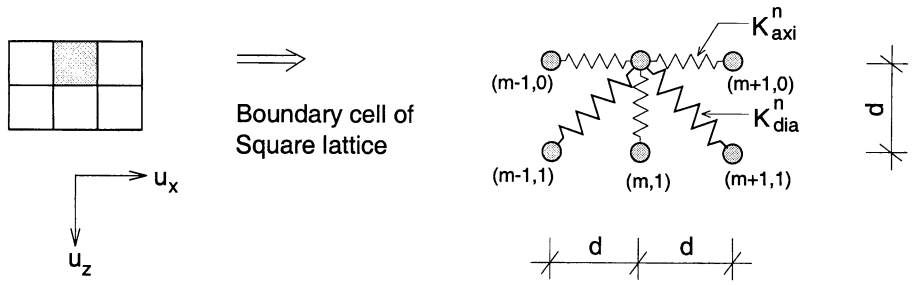

Fig. 3. Boundary cell of square lattice

In the long-wave approach, the equations of motion of the discrete model (1) should reduce to those of a standard elastic continuum (Born and Huang [1954], Maradudin et al. [1971], Kunin [1983], Suiker et al. [2000]). Accordingly, by taking the second-order Taylor approximation of (1) with respect to the displacements, we obtain the equations of motion in the long-wave limit

$$\begin{aligned} M\tilde{u}_{x,tt} &= (K_{axi}^n + K_{dia}^n)d^2\tilde{u}_{x,xx} + 2K_{dia}^n d^2\tilde{u}_{z,xz} + K_{dia}^n d^2\tilde{u}_{x,zz} \\ M\tilde{u}_{z,tt} &= (K_{axi}^n + K_{dia}^n)d^2\tilde{u}_{z,zz} + 2K_{dia}^n d^2\tilde{u}_{x,zx} + K_{dia}^n d^2\tilde{u}_{z,xx} \end{aligned} \tag{3}$$

where $,t$ is the partial derivative with respect to time. The tilde on top of the degrees of freedom designates their continuous character. Comparing (3) with the equations of motion for a classic elastic medium

$$\begin{aligned} \rho\tilde{u}_{x,tt} &= (\lambda + 2\mu)\tilde{u}_{x,xx} + (\lambda + \mu)\tilde{u}_{z,xz} + \mu\tilde{u}_{x,zz} \\ \rho\tilde{u}_{z,tt} &= (\lambda + 2\mu)\tilde{u}_{z,zz} + (\lambda + \mu)\tilde{u}_{x,zx} + \mu\tilde{u}_{z,xx} \end{aligned} \tag{4}$$

where λ and μ the Lamé constants and ρ the density, it becomes clear that (3) and (4) coincide if the following relations between the discrete micro-variables and the continuous macro-variables hold

$$
\begin{aligned}
M &= \rho d^3 \\
\frac{K^n_{axi} + K^n_{dia}}{d} &= \lambda + 2\mu \\
\frac{2K^n_{dia}}{d} &= \lambda + \mu \\
\frac{K^n_{dia}}{d} &= \mu
\end{aligned}
\tag{5}
$$

The anisotropic character of the lattice as a result of the different spring characteristics in axial and diagonal direction causes the equalities (5) to be unique only for the following condition: $K^n_{axi} = 2K^n_{dia}$. Substituting this constraint in (5) yields the Lamé constants

$$
\begin{aligned}
\lambda &= \frac{K^n_{axi}}{2d} \\
\mu &= \frac{K^n_{axi}}{2d}
\end{aligned}
\tag{6}
$$

As expression (6) illustrates, the long-wave limit of the discrete model reduces to the continuum model for the specific case $\lambda = \mu$, corresponding to a Poisson's ratio of $\nu = 0.25$. When extending the discrete model with more spring types (i.e. shear springs, rotational springs), the restriction on the Poisson's ratio will be released (Suiker et al. [2000]). However, the quality of the model results is not affected by such a constraint. Substituting $K^n_{axi} = 2K^n_{dia}$ in the equations of motion for the inner cell (1) gives

$$
\begin{aligned}
M\ddot{u}_x^{(m,n)} &= K^n_{axi}\Big[-3u_x^{(m,n)} + u_x^{(m+1,n)} + u_x^{(m-1,n)} \\
&\quad + \frac{1}{4}(u_x^{(m+1,n+1)} + u_x^{(m-1,n+1)} + u_x^{(m-1,n-1)} + u_x^{(m+1,n-1)}) \\
&\quad + \frac{1}{4}(u_z^{(m+1,n+1)} + u_z^{(m-1,n-1)} - u_z^{(m+1,n-1)} - u_z^{(m-1,n+1)})\Big] \\
M\ddot{u}_z^{(m,n)} &= K^n_{axi}\Big[-3u_z^{(m,n)} + u_z^{(m,n+1)} + u_z^{(m,n-1)} \\
&\quad + \frac{1}{4}(u_z^{(m+1,n+1)} + u_z^{(m+1,n-1)} + u_z^{(m-1,n-1)} + u_z^{(m-1,n+1)}) \\
&\quad + \frac{1}{4}(u_x^{(m+1,n+1)} + u_x^{(m-1,n-1)} - u_x^{(m+1,n-1)} - u_x^{(m-1,n+1)})\Big]
\end{aligned}
\tag{7}
$$

In the same manner, substituting the constraint in the equations of motion for the boundary cell (2) yields

$$
\begin{aligned}
M\ddot{u}_x^{(m,0)} &= \frac{1}{2}K^n_{axi}\Big[-5u_x^{(m,0)} + 2u_x^{(m+1,0)} + 2u_x^{(m-1,0)} + \frac{1}{2}u_x^{(m+1,1)} \\
&\quad + \frac{1}{2}u_x^{(m-1,1)} + \frac{1}{2}u_z^{(m+1,1)} - \frac{1}{2}u_z^{(m-1,1)}\Big] \\
M\ddot{u}_z^{(m,0)} &= \frac{1}{2}K^n_{axi}\Big[-3u_z^{(m,0)} + 2u_z^{(m,1)} + \frac{1}{2}u_z^{(m+1,1)} + \frac{1}{2}u_z^{(m-1,1)} \\
&\quad + \frac{1}{2}u_x^{(m+1,1)} - \frac{1}{2}u_x^{(m-1,1)}\Big]
\end{aligned}
\tag{8}
$$

Now, in order to solve (7), we will look for solutions of the harmonic form

$$\begin{aligned} u_x^{(m,n)} &= A\exp(i(\omega t - mk_x d - nk_z d)) \\ u_z^{(m,n)} &= B\exp(i(\omega t - mk_x d - nk_z d)) \end{aligned} \tag{9}$$

in which ω is the angular frequency, the imaginary number $i^2 = -1$, A and B are the wave amplitudes and k_x and k_z are the wave numbers in x-direction and z-direction, respectively. Combining (9) with (7) leads to

$$\begin{aligned} &A[M\omega^2 + K_{axi}^n(2\cos(k_x d) + \cos(k_x d)\cos(k_z d) - 3)] \\ &+ B[K_{axi}^n(-\sin(k_x d)\sin(k_z d))] = 0 \\ \\ &A[K_{axi}^n(-\sin(k_x d)\sin(k_z d))] \\ &+ B[M\omega^2 + K_{axi}^n(2\cos(k_x d) + \cos(k_x d)\cos(k_z d) - 3)] = 0 \end{aligned} \tag{10}$$

Via straightforward algebra, the relations (10) can be solved for the wave number k_z

$$\begin{aligned} k_z^{(1),(2)} &= \pm\frac{1}{d}\arccos\left(\frac{M\omega^2 + K_{axi}^n(\cos(k_x d) - 4)}{-K_{axi}^n(2\cos((k_x d) + 1))}\right) \\ k_z^{(3),(4)} &= \pm\frac{1}{d}\arccos\left(\frac{-M\omega^2 - K_{axi}^n(\cos(k_x d) - 2)}{K_{axi}^n}\right) \end{aligned} \tag{11}$$

In correspondence with the four solutions $k_z^{(j)}$, the amplitude vectors of the harmonic expressions (9) have four components: $A^{(j)} = \{A^{(1)}, A^{(2)}, A^{(3)}, A^{(4)}\}$ and $B^{(j)} = \{B^{(1)}, B^{(2)}, B^{(3)}, B^{(4)}\}$. The eigen vector that reflects the amplitude ratio $D^{(j)} = B^{(j)}/A^{(j)}$, results from combining (11) either with (10-a) or with (10-b), where the first combination yields

$$\begin{aligned} D^{(1),(2),(3),(4)} &= \frac{B^{(1),(2),(3),(4)}}{A^{(1),(2),(3),(4)}} \\ &= \left.\frac{M\omega^2 + K_{axi}^n(2\cos(k_x d) + \cos(k_x d)\cos(k_z d) - 3)}{K_{axi}^n\sin(k_x d)\sin(k_z d)}\right|_{k_z = k_z^{(1),(2),(3),(4)}} \end{aligned} \tag{12}$$

Invoking (9) and using (11}) and (12), we obtain a general expression for the free propagation of harmonic body waves

$$\begin{aligned} u_x^{(m,n)} &= (A^{(1)}\exp(-ink_z^{(1)}d) + A^{(2)}\exp(-ink_z^{(2)}d) + A^{(3)}\exp(-ink_z^{(3)}d) \\ &\quad + A^{(4)}(\exp -ink_z^{(4)}d))\exp(i(\omega t - mk_x d)) \\ \\ u_z^{(m,n)} &= (A^{(1)}D^{(1)}\exp(-ink_z^{(1)}d) + A^{(2)}D^{(2)}\exp(-ink_z^{(2)}d) \\ &\quad + A^{(3)}D^{(3)}\exp(-ink_z^{(3)}d) + A^{(4)}D^{(4)}\exp(-ink_z^{(4)}d))\exp(i(\omega t - mk_x d)) \end{aligned} \tag{13}$$

3 Formulation of the boundary value problem

In order to examine the boundary value problem that reflects the layer response to a moving load, four boundary conditions have to be formulated. At the top of the layer ($z = 0$), two boundary conditions follow from the dynamic balance of forces acting on the free boundary cell (8). This leads to

$$M\ddot{u}_x^{(m,0)} = \frac{1}{2}\hat{\kappa}_{axi}^n\left[-5u_x^{(m,0)} + 2u_x^{(m+1,0)} + 2u_x^{(m-1,0)} + \frac{1}{2}u_x^{(m+1,1)} + \frac{1}{2}u_x^{(m-1,1)} + \frac{1}{2}u_z^{(m+1,1)} - \frac{1}{2}u_z^{(m-1,1)}\right]$$

$$M\ddot{u}_z^{(m,0)} = \frac{1}{2}\hat{\kappa}_{axi}^n\left[-3u_z^{(m,0)} + 2u_z^{(m,1)} + \frac{1}{2}u_x^{(m+1,1)} + \frac{1}{2}u_z^{(m-1,1)} + \frac{1}{2}u_x^{(m+1,1)} - \frac{1}{2}u_x^{(m-1,1)}\right] + dF_z\delta(md - vt) \tag{14}$$

in which F_z is the magnitude of the vertical load and v is the load velocity. In (14-b), the load magnitude has been multiplied by the cell distance d (=particle diameter), which is necessary to provide the loading term with the same dimension as the remaining terms in this equation. Further, $\delta(..)$ is the Dirac delta function, and $\hat{\kappa}_{axi}^n$ is an operator of the form

$$\hat{\kappa}_{axi}^n = K_{axi}^n + C_{axi}^n\frac{d}{dt} \tag{15}$$

which is used instead of the longitudinal axial spring constant K_{axi}^n, in order to extend the discrete lattice with a longitudinal viscosity C_{axi}^n. In the same manner as the discrete stiffness K_{axi}^n is related to the Lamé constants λ and μ (Eq.(6)), the discrete viscosity C_{axi}^n is related to the corresponding macroscopic viscosity parameters λ^* and μ^*

$$\lambda^* = \frac{C_{axi}^n}{2d}$$
$$\mu^* = \frac{C_{axi}^n}{2d} \tag{16}$$

As we consider the layer support to be infinitely stiff, at the bottom of the layer ($z = nd = H$) the displacements in x- and z-direction are equal to zero

$$u_x^{(m,H/d)} = 0$$
$$u_z^{(m,H/d)} = 0 \tag{17}$$

The next step is to transform the four boundary conditions (14) and (17) to the Fourier domain. Accordingly, the necessary Fourier transforms with respect to time t are

$$
\begin{aligned}
\int_{-\infty}^{\infty} u_x^{(m,n)}(t)\exp(-i\omega t)dt &= U_x^{(m,n)}(\omega)\\
\int_{-\infty}^{\infty} \dot{u}_x^{(m,n)}(t)\exp(-i\omega t)dt &= i\omega U_x^{(m,n)}(\omega)\\
\int_{-\infty}^{\infty} \ddot{u}_x^{(m,n)}(t)\exp(-i\omega t)dt &= -\omega^2 U_x^{(m,n)}(\omega)\\
\int_{-\infty}^{\infty} u_z^{(m,n)}(t)\exp(-i\omega t)dt &= U_z^{(m,n)}(\omega)\\
\int_{-\infty}^{\infty} \dot{u}_z^{(m,n)}(t)\exp(-i\omega t)dt &= i\omega U_z^{(m,n)}(\omega)\\
\int_{-\infty}^{\infty} \ddot{u}_z^{(m,n)}(t)\exp(-i\omega t)dt &= -\omega^2 U_z^{(m,n)}(\omega)\\
\int_{-\infty}^{\infty} dF_z\delta(md-vt)\exp(-i\omega t)dt &= \frac{dF_z}{v}\exp\left(\frac{-i\omega md}{v}\right)
\end{aligned}
\tag{18}
$$

which turns the boundary conditions (14) and (17) into

$$
\begin{aligned}
&M\omega^2 U_x^{(m,0)} + \frac{1}{2}\hat{\kappa}_{axi}^n\Big[-5U_x^{(m,0)} + 2U_x^{(m+1,0)} + 2U_x^{(m-1,0)} + \frac{1}{2}U_x^{(m+1,1)}\\
&\qquad + \frac{1}{2}U_x^{(m-1,1)} + \frac{1}{2}U_z^{(m+1,1)} - \frac{1}{2}U_z^{(m-1,1)}\Big] = 0\\
&M\omega^2 U_z^{(m,0)} + \frac{1}{2}\hat{\kappa}_{axi}^n\Big[-3U_z^{(m,0)} + 2U_z^{(m,1)} + \frac{1}{2}U_z^{(m+1,1)} + \frac{1}{2}U_z^{(m-1,1)}\\
&\qquad + \frac{1}{2}U_x^{(m+1,1)} - \frac{1}{2}U_x^{(m-1,1)}\Big] = -d\frac{F_z}{v}\exp\left(\frac{-i\omega md}{v}\right)
\end{aligned}
$$

$$
\begin{aligned}
U_x^{(m,H/d)} &= 0\\
U_z^{(m,H/d)} &= 0
\end{aligned}
\tag{19}
$$

The Fourier boundary conditions (19) can be met by Fourier displacements of the form

$$
\begin{aligned}
U_x^{(m,n)} &= \left(A^{(1)}\exp(-ink_z^{(1)}d) + A^{(2)}\exp(-ink_z^{(2)}d) + A^{(3)}\exp(-ink_z^{(3)}d)\right.\\
&\quad \left. + A^{(4)}\exp(-ink_z^{(4)}d)\exp(-im\bar{k}_x d)\right|_{\bar{k}_x=\frac{\omega}{v}}\\
U_z^{(m,n)} &= \left(A^{(1)}D^{(1)}\exp(-ink_z^{(1)}d) + A^{(2)}D^{(2)}\exp(-ink_z^{(2)}d)\right.\\
&\quad + A^{(3)}D^{(3)}\exp(-ink_z^{(3)}d) + \left.A^{(4)}D^{(4)}\exp(-ink_z^{(4)}d)\right)\exp(-im\bar{k}_x d)\Big|_{\bar{k}_x=\frac{\omega}{v}}
\end{aligned}
\tag{20}
$$

Because in the z-direction the solution (20) has the same form as the solution for free body wave propagation (see Eq.(13)), correspondingly, the wave numbers $k_z^{(i)}$ follow from (11), and the amplitude ratios $D^{(i)}$ follow from (12) with K_{axi}^n being replaced by the 'complex stiffness' $K_{axi}^n + i\omega C_{axi}^n$. In the x-direction, however, the wave number $\bar{k}_x$ is dictated by the moving load; $\bar{k}_x = \omega/v$, where the bar on top of the wave number indicates its "forced" character.

Substituting the Fourier displacements (20) into the Fourier boundary conditions (19) gives

$$
\begin{aligned}
&[A^{(1)} + A^{(2)} + A^{(3)} + A^{(4)}]\left(M\omega^2 + \frac{1}{2}(K^{n}_{axi} + i\omega C^{n}_{axi})(4\cos(\bar{k}_x d) - 5)\right) \\
&\quad + [A^{(1)}\exp(-ik_z^{(1)}d) + A^{(2)}\exp(-ik_z^{(2)}d) + A^{(3)}\exp(-ik_z^{(3)}d) \\
&\quad + A^{(4)}\exp(-ik_z^{(4)}d)]\frac{1}{2}(K^{n}_{axi} + i\omega C^{n}_{axi})\cos(\bar{k}_x d) \\
&\quad + [A^{(1)}D^{(1)}\exp(-ik_z^{(1)}d) + A^{(2)}D^{(2)}\exp(-ik_z^{(2)}d) + A^{(3)}D^{(3)}\exp(-ik_z^{(3)}d) \\
&\quad + A^{(4)}D^{(4)}\exp(-ik_z^{(4)}d)]\left(-\frac{1}{2}(iK^{n}_{axi} - \omega C^{n}_{axi})\sin(\bar{k}_x d)\right)\Big|_{\bar{k}_x = \frac{\omega}{v}} = 0 \\
&[A^{(1)}D^{(1)} + A^{(2)}D^{(2)} + A^{(3)}D^{(2)} + A^{(4)}D^{(4)}]\left(M\omega^2 - \frac{3}{2}(K^{n}_{axi} + i\omega C^{n}_{axi})\right) \\
&\quad + [A^{(1)}D^{(1)}\exp(-ik_z^{(1)}d) + A^{(2)}D^{(2)}\exp(-ik_z^{(2)}d) + A^{(3)}D^{(3)}\exp(-ik_z^{(3)}d) \\
&\quad + A^{(4)}D^{(4)}\exp(-ik_z^{(4)}d)]\left(\frac{1}{2}(K^{n}_{axi} + i\omega C^{n}_{axi})(\cos(\bar{k}_x d) + 2)\right) \\
&\quad + [A^{(1)}\exp(-ik_z^{(1)}d) + A^{(2)}\exp(-ik_z^{(2)}d) + A^{(3)}\exp(-ik_z^{(3)}d) \\
&\quad + A^{(4)}\exp(-ik_z^{(4)}d)]\left(-\frac{1}{2}(iK^{n}_{axi} - \omega C^{n}_{axi})\sin(\bar{k}_x d)\right)\Big|_{\bar{k}_x = \frac{\omega}{v}} = -\frac{dF_z}{v} \\
&A^{(1)}\exp(-ik_z^{(1)}H) + A^{(2)}\exp(-ik_z^{(2)}H) + A^{(3)}\exp(-ik_z^{(3)}H) \\
&\quad + A^{(4)}\exp(-ik_z^{(4)}H)\big|_{\bar{k}_x = \frac{\omega}{v}} = 0 \\
&A^{(1)}D^{(1)}\exp(-ik_z^{(1)}H) + A^{(2)}D^{(2)}\exp(-ik_z^{(2)}H) + A^{(3)}D^{(3)}\exp(-ik_z^{(3)}H) \\
&\quad + A^{(4)}D^{(4)}\exp(-ik_z^{(4)}H)\big|_{\bar{k}_x = \frac{\omega}{v}} = 0
\end{aligned}
\tag{21}
$$

The system of equations (21) can be written in a matrix-vector form as

$$
E^{(i,j)}A^{(j)}\big|_{\bar{k}_x = \frac{\omega}{v}} = F^{(i)} \tag{22}
$$

where $E^{(i,j)}$ is the 4 × 4 matrix that governs the eigen behaviour of the discrete layer, $A^{(j)} = \{A^{(1)}, A^{(2)}, A^{(3)}, A^{(4)}\}$ is the wave amplitude vector and $F^{(i)} = \{0, -dF_z/v, 0, 0\}$ is the force vector. Further, the repeated superscript "j" implies a summation. The amplitude vector can be found by employing Cramers rule

$$
A^{(j)} = \frac{\Delta_j}{\Delta} \tag{23}
$$

where, for a given set of elastic parameters, $\Delta = \Delta(\omega, \bar{k}_x, H, d)$ is the determinant of the eigen matrix $E^{(i,j)}$ with $\bar{k}_x = \frac{\omega}{v}$ being substituded, and Δ_j is the determinant of the eigen matrix with the j-th column being replaced by the force vector $F^{(i)}$. When the amplitude vector is calculated and substituted into (20), the steady state solution $\{u_x^{(m,n)}, u_z^{(m,n)}\}$ of the boundary value problem results from inverse Fourier transformation of (20), i.e.

$$
\begin{aligned}
u_x^{(m,n)}(t) &= \frac{1}{2\pi}\int_{-\infty}^{\infty} U_x^{(m,n)}(\omega)\exp(i\omega t)d\omega \\
u_z^{(m,n)}(t) &= \frac{1}{2\pi}\int_{-\infty}^{\infty} U_z^{(m,n)}(\omega)\exp(i\omega t)d\omega
\end{aligned}
\tag{24}
$$

The integrals (24) can be evaluated either by using complex contour integration, or by using direct numerical integration. In the current study we have chosen for numerical integration, as for realistic viscosity values of the ballast, the integrand (24) converges relatively fast. Also, the viscosity removes the integrand singularities emerging at the frequencies of the waves radiated by the load. In the next section we will discuss the steady state solutions (24) for various cases.

4 Discussion of results

For the parametric study in this section, we have used an axle load of F_z =200 kN, which is a common design value for railway lines in Holland. The ballast is assigned a Young's modulus E = 200 MPa, and a Poisson's ratio ν = 0.25 (corresponding to Lamé constants $\lambda = \mu$ =80 MPa). Furthermore, the ballast density is assumed as $\rho = 1800\ \mathrm{kg/m^3}$, while the layer thickness equals H = 300 mm. By using Eqs.(5) and (6), the macroscopic material parameters above can be transformed into microscopic material parameters for the discrete model. In order to examine the influence of the particle size, we will consider two different particle radii: $r = 0.5d$ = 1 mm and $r = 0.5d$ = 25 mm. The large particle size is realistic for ballast particles in common railway tracks (Selig and Waters [1994]).

Fig. 4 shows the vertical displacement u_z at $0.2H$ (=60 mm) below the surface, for a small particle radius r = 1 mm and a load velocity v = 150 km/h. The response has been computed for two different viscosities: $\mu^* = \lambda^* = 1 \times 10^3\ \mathrm{Ns/m^2}$ and $\mu^* = \lambda^* = 50 \times 10^3\ \mathrm{Ns/m^2}$. Due to the small particle size, the displacement pattern of the discrete layer approaches that of a continuum layer. For the small viscosity the response is symmetric, while for the large viscosity the response is slightly asymmetric. Naturally, a higher viscosity leads to a smaller maximum displacement.

When the particle radius is increased to r = 25 mm, for a relatively small viscosity $\mu^* = 1 \times 10^3\ \mathrm{Ns/m^2}$ considerable waves are radiated behind the load (Fig.5). This wave radiation is the result of the periodic inhomogeneous character of the discrete structure. More specifically, the emitted radiation is generated by individual particle motions, where the intensity of the radiation depends on the ratio between the load velocity and the particle size; v/d. For an increasing (*decreasing*) ratio v/d, the individual particle motions become less (*more*) intense, causing the discrete layer to respond more (*less*) like a continuum. Because the radiation is formed by higher harmonics, it is damped for a higher viscosity $\mu^* = 50 \times 10^3\ \mathrm{Ns/m^2}$. It can be further noticed that for the high viscosity, the maximum displacement is smaller than that for a smaller particle size of r = 1 mm (see Fig.4). This is, because for a given macroscopic stiffness, a greater particle size enlarges the local contact stiffness (see expression (6)), which thus leads to a decrease of the local peak.

The fact that a higher load velocity yields a reduction of the wave radiation, can be illustrated by increasing the load velocity to v = 300 km/h (Fig.6). Apparently, the radiation is lower than in Fig. 5, which is because a higher load velocity activates higher harmonics that are more easily damped by the particle viscosity. Further, the influence by a larger damping on the disappearance of the wave radiation is also apparent. Nevertheless, the damped response shows a larger maximum displacement than in Fig. 5, which is due to increased dynamic effects caused by the higher load velocity.

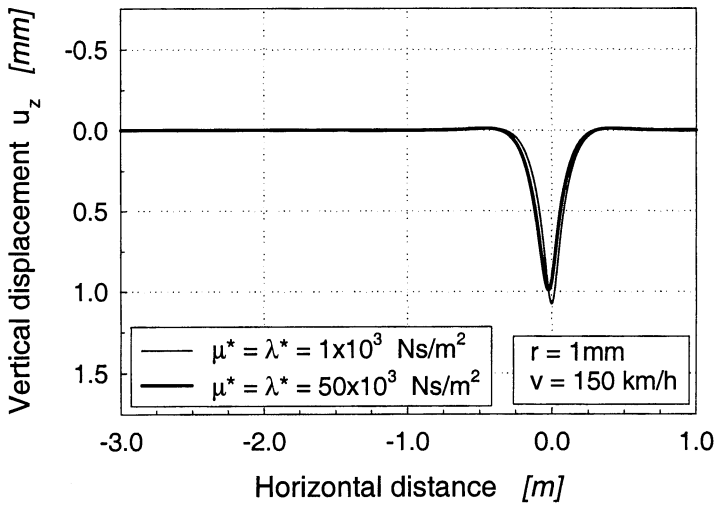

Fig. 4. Steady state displacement u_z at $z = 0.2H$ below the layer surface, for a load velocity $v = 150$ km/h, a particle radius $r = 1$ mm, and viscosities $\mu^* = \lambda^* = 1 \times 10^3$ Ns/m^2, $\mu^* = \lambda^* = 50 \times 10^3$ Ns/m^2.

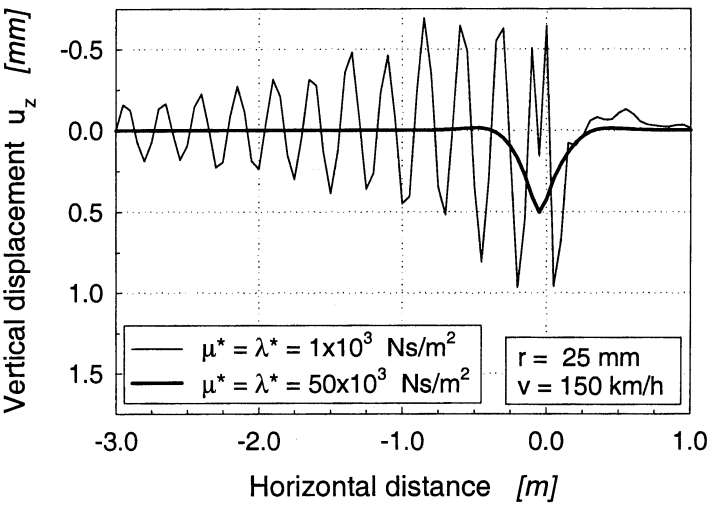

Fig. 5. Steady state displacement u_z at $z = 0.2H$ below the layer surface, for a load velocity $v = 150$ km/h, a particle radius $r = 25$ mm, and viscosities $\mu^* = \lambda^* = 1 \times 10^3$ Ns/m^2, $\mu^* = \lambda^* = 50 \times 10^3$ Ns/m^2.

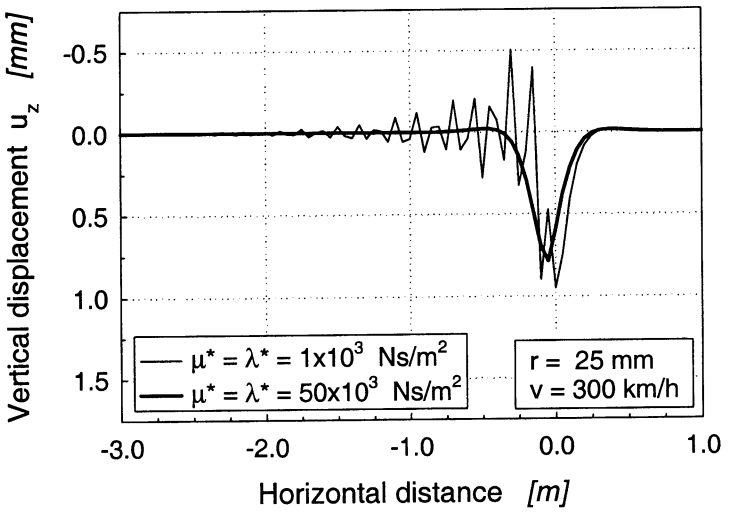

Fig. 6. Steady state displacement u_z at $z = 0.2H$ below the layer surface, for a load velocity $v = 300$ km/h, a particle radius $r = 25$ mm, and viscosities $\mu^* = \lambda^* = 1 \times 10^3$ Ns/m^2, $\mu^* = \lambda^* = 50 \times 10^3$ Ns/m^2.

5 Conclusions

In this paper, the response of a layer of discrete particles to a moving load has been analysed. This model is representative for the behaviour of a railroad ballast layer resting on a much stiffer substratum (e.g. a concrete railway bridge or railway foundation). After deriving the governing equations for the discrete model, the boundary value problem has been formulated and solved, thereby considering various parameter combinations. It has been demonstrated that for a particle radius $r =$ 25 mm, which is realistic for ballast particles in ordinary railway tracks, the response considerably differs from that of a continuum layer. Depending on the magnitude of the viscosity, particle perturbations may initiate wave radiation behind the moving load. The oscillating character of this wave radiation can have a deteriorating effect on the ballast layer, as it stimulates grinding and flattening of ballast particles, as well as loosening of the ballast packing structure. The decrease of wave radiation by an increased viscosity has been demonstrated. Hence, for reducing track maintenance and ballast replacement at railroad bridges and tunnels, it is recommendable to use ballasts with a considerably large damping capacity.

References

BORN, M. and HUANG, K. [1954], *Dynamical Theory of Crystal Lattices*, Clarendon Press, Oxford.

DIETERMAN, H.A. and METRIKINE, A. [1996], The equivalent stiffness of a half space interacting with a beam. Critical velocities of a moving load along the beam, *Eur. J. Mech. A/Solids*, **15**, pp. 67-90.

DIETERMAN, H.A. and METRIKINE, A. [1997], Critical velocities of a harmonic load moving uniformly along an elastic layer, *J.Appl. Mech. (ASME)*, **64**, pp. 596-600.

FRYBA, L.J. [1972], *Vibration of Solids and Structures under Moving Loads*, Noordhoff International Publishing, Groningen.

KUNIN, I.A. [1983], *Elastic Media with Microstructure, Vol. 2, Threedimensional Models*, Springer, Berlin.

LABRA, J.J. [1975], An axially stressed railroad track on an elastic continuum subjected to a moving load, *Acta Mech.*, **22**, pp. 113-129.

MARADUDIN, A.A., MONTROLL, E.M., WEISS, G.H., and IPATOVA, I.P. [1971], *Theory of Lattice Dynamics in the Harmonic Approximation*, Solid State Physics, Suppl. 3, Academic, New York.

SELIG, E.T. and WATERS, J.M. [1994], *Track Geotechnology and Substructure Management*, Thomas Telford Services Ltd, London.

SUIKER, A.S.J., CHANG, C.S., DE BORST, R., and ESVELD, C. [1999a], Surface waves in a stratified half space with enhanced continuum properties – Part 1 – Formulation of the boundary value problem, *Eur. J. Mech. A/Solids*, **18**, pp. 749-768.

SUIKER, A.S.J., CHANG, C.S., DE BORST, R., and ESVELD, C. [1999b], Surface waves in a stratified half space with enhanced continuum properties – Part 2 – Analysis of the wave characteristics in regard to high-speed railway tracks, *Eur. J. Mech. A/Solids*, **18**, pp. 769-784.

SUIKER, A.S.J., DE BORST, R., and ESVELD, C. [1998], Critical behaviour of a Timoshenko beam-half plane system under a moving load, *Arch. Appl. Mech*, **68**, pp. 158-168.

SUIKER, A.S.J., METRIKINE, A.V., and DE BORST, R. [2000], Comparison of wave propagation characteristics of the Cosserat continuum model and corresponding discrete lattice models, *Int. J. Solids Struct.*, accepted for publication.